COBEM 2021 26th International Congress of Mechanical Engineering
November 22-26, 2021, Virtual Congress, Brazil

COB-2021-0398
NUMERICAL ANALYSIS OF FLOW IN A SUPERSONIC SEPARATOR NOZZLE WITH CENTRAL BODY

Thomaz Garcia Faccioli
Reinaldo Marcondes Orselli, Ph.D.
Universidade Federal do ABC, centro de engenharia, modelagem e ciências sociais aplicadas, Avenida dos Estados, 5001, Santo André, SP, Brazil.
thomaz.faccioli@aluno.ufabc.edu.br
reinaldo.orselli@ufabc.edu.br

Ricardo Galdino da Silva, Ph.D.
Instituto de Aeronáutica e Espaço, departamento de ciência aeroespacial e tecnologia, Praça Marechal Eduardo Gomes, 50, São José dos Campos, SP, Brazil.
ri_galdino@yahoo.com.br

Bruno do Carmo Souza, Ph.D.
Universidade de São Paulo, Escola Politécnica, departamento de engenharia mecânica, São Paulo, SP, Brazil.
bruno.carmo@usp.br

Abstract. *The aim of this study is to carry out numerical simulations of a supersonic separator in order to investigate the main physical characteristics of this device with central body, analyzing features such as shock wave topology and position and separation efficiency. For the numerical analyzes, the device is considered axisymmetric with a central body and a collector. In addition, the centrifugation effect is made by imposing a swirling flow at the nozzle inlet. For the simulations, both single component and multi component gas are taken into account, with the use of methane gas as well as mixtures with CO_2 and air in different concentrations. In general, considering a fixed supersonic nozzle geometry, keeping the same length and area ratio, it is noted that the swirl intensity combined with the collector position are key features to set the flow to be able to perform the separation of heavier components, such as CO_2.*

Keywords: *Computational Fluid Dynamics, Natural gas, Shock wave, Supersonic separator.*

1. INTRODUCTION

Due to the rising world energy demand along with the necessity to reduce the environmental impact that the current processes of energy production involve, the development of new technological solutions to minimize emission of greenhouse gases and optimize the energy sources exploration has become more compelling. Therefore, natural gas has turned into a great alternative to compose the energy matrix of several countries, as, in comparison to others traditional fossil fuels, it has a lower emission of gases harmful to the environment. Since one of the main environmental goals is reducing the emission of CO_2 gases in the atmosphere, according to Da Silva (2010), natural gas emits about 20 to 30% less CO_2 gases less compared to fuel oil and 40 to 50% less than solid fuels, such as coal.

Natural gas is essentially a mixture of hydrocarbons in gaseous form, which its mainly concentration is methane (CH_4). Some of the other components, such as CO_2, must be removed as long as the presence of this composing reduces heating value of the natural gas and it causes corrosion of the pipes and hence corrosion-resistant materials have to be used which leads to a costly facility (Altam *et al.*, 2017). Thus, it is necessary to develop a compact equipment capable of purifying the natural gas directly at offshore platforms so its transport and commercialization can be more efficient.

In this context, there is a new proposed technology known as supersonic separator that uses the processes of expansion to cool and condensate the heavier components, such as CO_2, allowing the liquid part to be separated from the gas by centrifugation. Regarding the challenges and demands set out above, this device has several advantages compared to other traditional arrangement, such as membrane permeation and chemical absorption: it has no moving parts, it does not operate with chemical products, it is very compact, it does not require manual operation, it has low weight and cost, less maintenance and, in operational terms it is energetically more efficient (Liu *et al.*, 2014; Arinelli, 2015).

As shown in Figure 1, the concept of supersonic separator is composed of a Laval nozzle, a cyclonic separation section and a diffuser. The fluid is accelerated in the convergent section of the Laval nozzle, then, becoming supersonic in the divergent section. There, the gas expands causing a decrease in the static pressure and temperature. As such, water and heavy hydrocarbons are condensed in the divergent section which are carried towards the wall due to the centrifugation imposed, and finally removed through the collector.

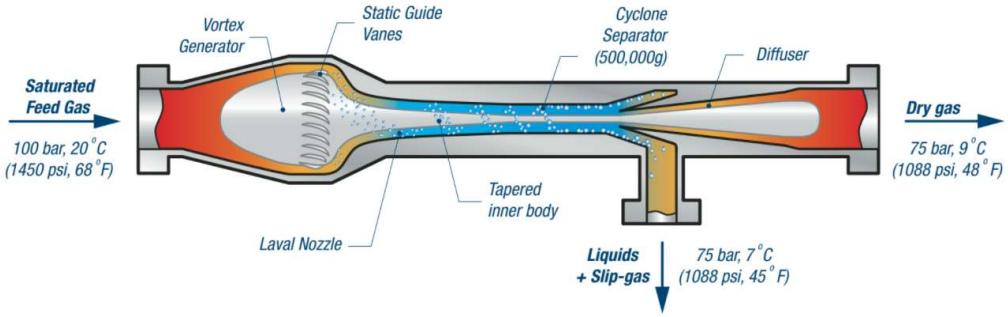

Figure 1. Cross-section of a supersonic device developed by Twister BV with typical process conditions (Twister BV, 2017).

As the flow in a supersonic separator has complex operating conditions with high velocity and pressure gradients coupled with formation of shock waves and consequent interactions with the boundary layer, there is a need to carry out careful studies regarding such issues, evaluating the flow behavior as well as optimizing the system. For this purpose, numerical simulations are performed to give a better understanding of the behavior of the flow in a simplified model of a supersonic separator. In addition, the capability of such numerical simulations to predict and deal with a such complex flow observed in this device is analyzed, for example, with the presence of shock wave, boundary layer interaction, flow separation, gas mixture and centrifugation.

The aim of this work is to perform numerical simulations of the flow through an axisymmetric model representing the supersonic separator with a particular geometry based on the device established by Twister BV, which has a central body. As illustrated in Figure 1, the central body has the function of making more efficient the induced swirl, allowing the condensed particles to be carried towards the collector.

2. METHODOLOGY

The commercial code ANSYS Fluent is used for the CFD numerical simulations, which is based on the Finite Volume method to solve the governing equations of the fluid mechanics. The continuity, momentum, and energy equation are expressed in Eqs. (1), (2) and (3).

$$\frac{\partial \rho}{\partial t} + \nabla \cdot (\rho U) = 0, \tag{1}$$

$$\frac{\partial \rho U}{\partial t} + \nabla \cdot (\rho U U) - \nabla \cdot \mu \nabla \cdot U = -\nabla p, \tag{2}$$

$$\frac{\partial \rho e}{\partial t} + \nabla \cdot (\rho U e) - \nabla \cdot \left(\frac{k}{C_v}\right) \nabla \cdot e = p \nabla U, \tag{3}$$

where ρ, U, p are the gas density, velocity, and pressure, respectively. μ is the dynamic viscosity; C_v is the specific heat at constant volume; e is the specific internal energy; k is the total kinetic energy per unit mass; t is the time.

The pressure-based solver is employed to solve the equations. In this algorithm the pressure equation is derived from the continuity and the momentum equations in such a way that the velocity field, corrected by the pressure, satisfies the continuity (Ansys Inc, 2019). Besides that, for the coupling of the velocity field and pressure, it was applied the SIMPLE algorithm in which the relationship between velocity and pressure corrections is used to impose mass conservation and to determinate the pressure field. Additionally, for the spatial discretization, the second-order upwind scheme is adopted for all flow variables. Alternatively, for the simulation considering swirl, the PRESTO! (PREssure STaggering Option) scheme is applied for the pressure interpolation. The PRESTO! scheme uses the discrete continuity equation for a "staggered" control volume about the face to determinate the "staggered" pressure.

As the numerical solution is obtained through an iterative method, a convergence criterion is used. Therefore, a measure called residual is calculated for each iteration, which represents the conservation of the flow properties, and its value should decrease along the simulation as the numerical results approximates to the solution. For all simulations the convergence criterion established is set to at least a maximum residual value of 1e-3 for all transport equations, and 1e-6 for the energy transport equation, as recommended for an accurate numerical solution by Ansys Inc (2019).

For the numerical simulations, the flow is considered to behave as steady. In order to deal with the high turbulent flow, and its inherent broad range of turbulent scales, the RANS (Reynolds Averaged Navier-Stokes) equations approach is used to model the turbulent motion. The RANS equations are based on the time-averaged Navier-Stokes equations, in which the turbulent flow is characterized in terms of the mean value of flow property and some statistical properties of

their temporal fluctuations (Versteeg & Malalaskera, 2007). The application of the time-averaged Navier-Stokes equations results in a non-linear term dependent on the fluctuating part of the flow velocities, which is known as the Reynolds stress tensor. In order to close the RANS equations with the unknown Reynolds stress tensor, additional transport equations are proposed as turbulence models that represent the behavior of the Reynolds stress tensor linked to time-average flow quantities. For this purpose, the Boussinesq hypothesis is used to relate the fluctuating terms with the mean flow for Reynolds stress tensor (Versteeg & Malalaskera, 2007). Some proposed models based on the Boussinesq hypothesis involves additional variables to statistically quantify the fluctuating component, such as the turbulence kinetic energy (k) and its dissipation represented by "Epsilon" (ε) or "Omega" (ω), the specific rate of dissipation of turbulence. For this work, the two-equation model k-ε RNG is used, which is derived using a statistical technique called renormalization group theory, based on the hypothesis that the effects of molecular viscosity are negligible and the flow is entirely turbulent (Yakot *et al.*, 1992). Additionally, for the numerical simulations considering swirling flow, the k-ω SST model (Menter, 1994) is used, which is a hybrid model using a transformation of the k-ε model into a k-ω model in the near-wall region and the standard k-ε model in the fully turbulent region far from the wall (Versteeg & Malalaskera, 2007).

For the numerical simulations, besides considering the gas as compressible to behave as an ideal gas (equation of state), since the supersonic separator works at a critical temperature and pressure range, the Redlich-Kwong real gas model is also used to consider this effect. The Redlich-Kwong model (Redlich and Kwong, 1949) is an analytic cubic equation of state with a relatively simple form.

In addition, since the aim of this work is to carry out a preliminary study of the flow through a simplified axisymmetric supersonic separator model, the condensation effects on the flow are not contemplate in the numerical simulations.

2.1 Geometry and Mesh

As shown in Figure 2, the geometry considered as axisymmetric for the numerical simulations is based on the published works of Cao and Yang (2015) and Wen *et al.* (2011), who studied the performance of supersonic separator. This geometry has a particular feature with a central body with an ellipsoidal shape at the upstream side. The tunnel bounded by the wall and the central body forms a convergent-divergent Laval nozzle. As observed in Figure 2, just upstream the throat there is a section known as cyclonic separation, where the flow is supersonic, that ends at the collector entrance, following that there is the diffuser section up to the main flow outlet.

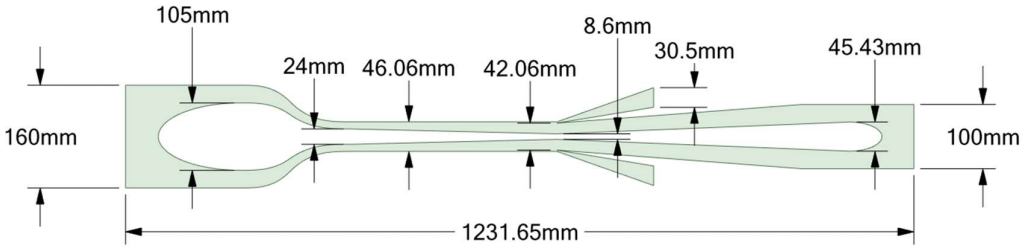

Figure 2. Mirrored cross-section of the axisymmetric supersonic separator design considered.

The diameter of the wall and central body in the convergent section of the Laval nozzle, where the fluid is accelerated up to sonic speed at the throat, are described by Eq. 4.

$$\begin{cases} \frac{D-D_{cr}}{D_1-D_{cr}} = 1-\frac{1}{X_m^2}\left(\frac{x}{L}\right)^3 & for\ \left(\frac{x}{L} \le X_m\right) \\ \frac{D-D_{cr}}{D_1-D_{cr}} = \frac{1}{(1-X_m)^2}\left(1-\frac{x}{L}\right)^3 & for\ \left(\frac{x}{L} > X_m\right) \end{cases}, \tag{4}$$

where D_1, D_{cr} and L are the inlet diameter, the throat diameter and the convergent section length, respectively. X_m is the relative coordinate of this convergent curve set 0.45 and D is the diameter for a certain value of x.

As shown in Figure 2, across the convergent-divergent section of the nozzle the fluid is accelerated and becomes supersonic downstream the throat. In the divergent section, the supersonic flow accelerates and expands, as a result the static pressure and temperature drops, which allows the condensation of some heavier components mixed within the natural gas, such as CO_2. By imposing centrifugation, the condensed particles formed are carried towards the upper wall and are captured by a collector attached to the wall. Finally, downstream the collector, the remaining part of the gas reaches the diffuser section which has a role to slow the incoming gas and recover the pressure up to the device outlet.

For the numerical simulations, a structured mesh was generated with a total of 77160 volumes. Due to the high velocity gradient formed in the shock wave and boundary layer region, the mesh was refined in the beginning region of the diffuser

section, around the separator walls and the central body. The mesh displayed in Figure 3 was built with the software ANSYS Meshing.

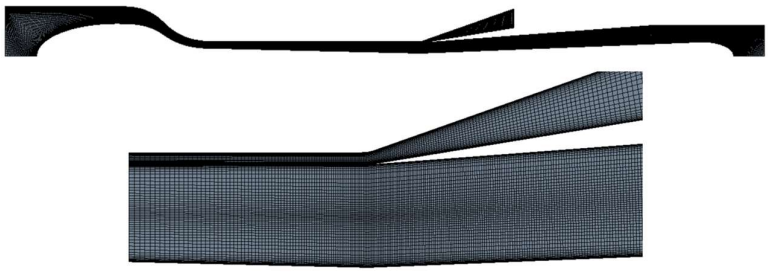

Figure 3. Computational mesh for the axisymmetric simulations, an extended view is shown at the bottom of the figure.

For the mesh generated, the y^+, non-dimensional distance of the first cell adjacent to the wall is set in the range of 20 to 300 in order to solve the flow gradients on the wall region and not to present a high number of cells and consequently a high computational cost of simulation. Additionally, in order to resolve the flow gradients on the boundary layer, and dealing with the broad range of y^+ values, a near-wall treatment known as 'enhanced wall treatment' in ANSYS Fluent is used. This model uses a damping function to blend the separate models in the two-layer approach and make the transition between the a near wall model for the viscous sublayer region be smoother (Ansys Inc, 2019). In addition, the enhanced turbulent law-of-the-wall for compressible flow with heat transfer and pressure gradients is considered in the setup of the enhanced wall treatment.

In order to verify the grid sensitivity to the results, a grid independency study was performed by means of a coarse, medium and fine mesh with 37011, 77160 and 152551 cells, respectively. As observed in Fig. 4 with the static temperature values along the centerline, line formed by equidistant points from the separator and central body walls, there is not a noticeable difference with the values of static temperature with the three mesh refinements considered. A similar behavior was also observed for the other main variables all over the computational domain, as such the presented results are not influenced by the mesh refinement.

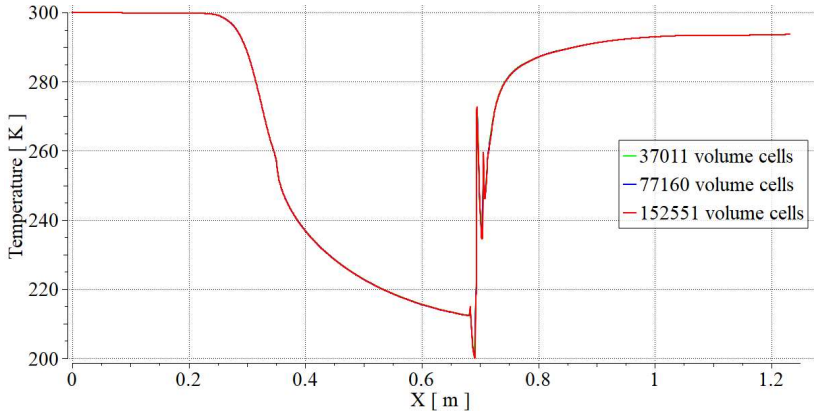

Figure 4. Static temperature values along the centerline of the flow in the supersonic separator with three different mesh refinements, 37011, 77160 and 152551 volume cells.

2.2 Boundary Conditions

The parameters imposed in this study were based on the typical working conditions of the supersonic separator available in the literature. The total pressure and temperature applied at the inlet are 40.00171 bar and 300 K. The static pressure at collector and nozzle outlets are set in such a way that a first the shock wave is located at the entrance already inside the collector and a second shock wave just downstream the collector at the beginning region of the diffuser section. For this, the static pressure at the collector and diffuser outlets imposed for the numerical simulations are 16 bar and 26 bar, respectively. The static temperature of both outlet sections is 300 K as well as at the inlet section. For the turbulence parameters, the turbulence intensity and the viscosity ratio are set as 0.035 and 1 for the inlet, and 0.042 and 4 for the outlet, respectively. Adiabatic no-slip wall is adopted at the separator wall and central body and symmetry condition for the axis line.

3. RESULTS AND DISCUSSION

Following the numerical set-up as aforementioned in section 2.0, with respect to the numerical simulation carried out to obtain the flow field solution along the supersonic nozzle. At first, no swirl is considered and the methane gas is assigned as the fluid composition. Fig. 5, 6 and 7 shows the static pressure, static temperature and Mach number field in the supersonic separator, respectively. It can be seen from the figures that the flow reaches Mach 1 at the throat and is accelerated to supersonic velocity in the separation section reaching the maximum value of Mach 1.77. As a result, the static pressure and temperature decreases up to 7.5 bar and 198 K in this region, which promote the condensation of heavier components, such as CO_2.

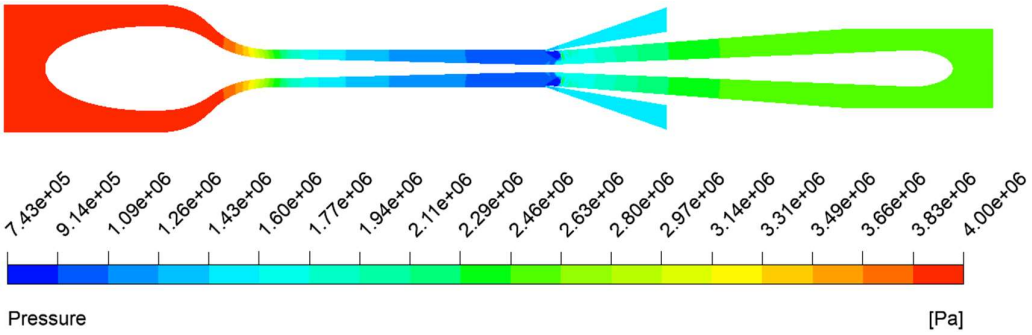

Figure 5. Static pressure field in the supersonic separator.

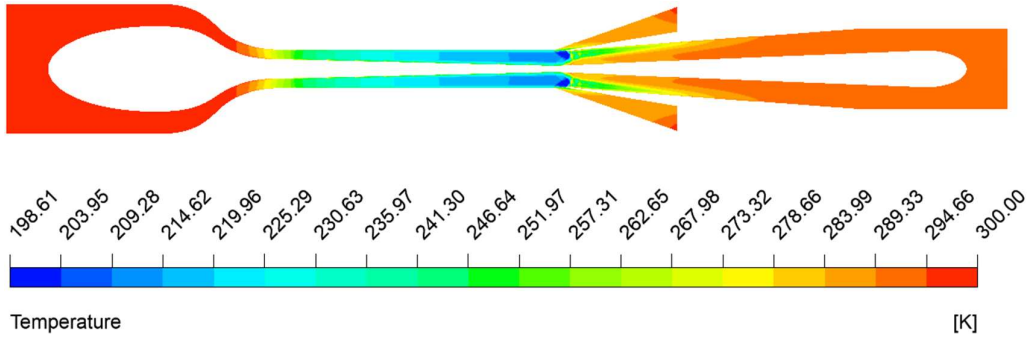

Figure 6. Static temperature field in the supersonic separator.

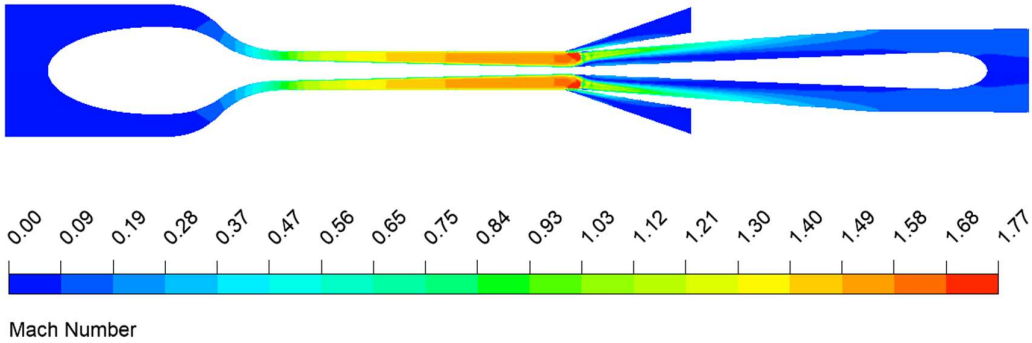

Figure 7. Mach number field in the supersonic separator.

In Figs. 5, 6 and 7, it is observed a Mach number higher than 1.6 just upstream of the shock wave. As the shock is strong enough to separate the boundary layer, the shock is bifurcated and one or more shocks appear downstream of the bifurcated shock (Matsuo *et. al*, 1999), which leads to a shock-train topology as observed in Fig. 7. As illustrated in Figs. 6 and 7, there is a massive flow separation just downstream the shock wave due to the high adverse pressure gradient through the shock wave train. Such flow separation leads to intense turbulent fluctuations that extends over the diffusor and collector, as shown in turbulence kinetic energy field illustrated in Fig. 8. It is noticed in Fig. 6, at the outlet of the

collector, an increase of the temperature, which is due to reversed flow associated with a flow separation downstream the shock wave.

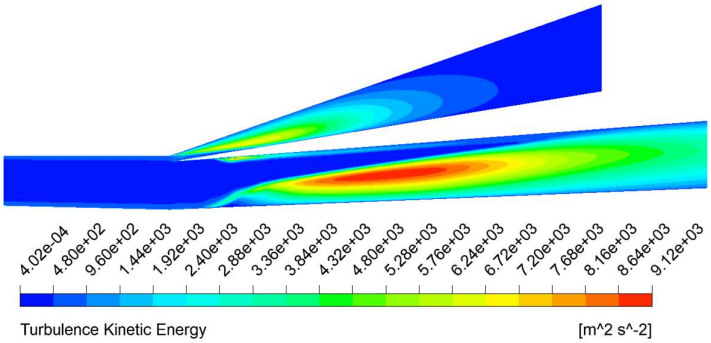

Figure 8. Turbulence kinetic energy field in an extended view of the shock waves region of the supersonic separator.

In order to verify the simulation convergence and to ensure the conservation of the flow properties, the residual values for each discretized transport equation are presented in Table 1. All residual for each transport equation is below 1e-3, and below 1e-6 for energy equation.

Table 1. Residual values of each algebraic discretized equation.

Continuity	x-velocity	y-velocity	Energy	k	Epsilon
7.8117e-05	2.3199e-06	1.0250e-06	1.6767e-07	1.1650e-06	8.9908e-05

3.1 Multicomponent gas simulation

The effects of CO_2 mixed with CH_4 and air in different concentrations in a supersonic separator is presented in this section. In addition, besides methane, air is also included in this study as its commonly used as a working gas in many references, such as in Wang and Hu (2018) and Yang *et al.* (2014). Respectively, Fig. 9 and 10 shows the static temperature and velocity variation along the centerline of the flow through the supersonic separator axisymmetric model (Fig. 2).

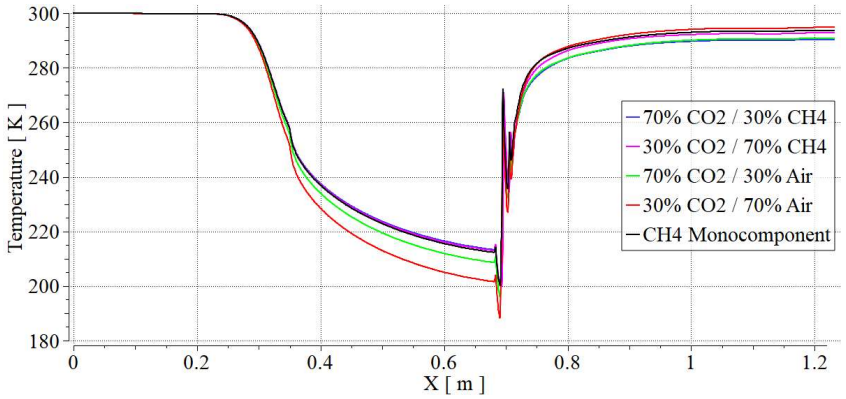

Figure 9. Static temperature variation along the centerline of the flow in the supersonic separator.

Observing Fig. 9, it can be noticed that the static temperature curves for the simulations considering CO_2 and CH_4 mixture are quite similar, since their heat capacity ratios (γ) values are very close, 1.289 for CO_2 and 1.299 for CH_4 (Van Wylen, 1998). Otherwise, the heat capacity ratio of air is 1.400, justifying the lower temperature reached by the fluid with the highest fraction of air. Furthermore, the shock wave position is unaffected by the gas composition change, possibly because the heat capacity values of these three gases are not very different, not enough to modify the shock wave position.

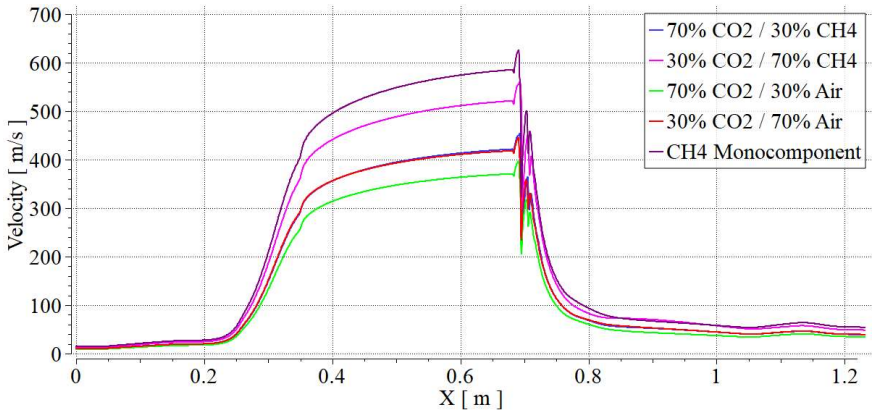

Figure 10. Velocity magnitude along the centerline of the flow in a supersonic separator.

According to the Fig. 10, it is noticed that as the CO_2 concentration molar fraction increases, in both mixtures methane and air, the flow velocity decreases. Since the density of CO_2 is 1.775 kg/m^3, CH_4 is 0.648 kg/m^3 and air is 1.169 kg/m^3, the increment of carbon dioxide in the mass fraction results in an increase of the density of the two mixtures. As the necessary energy to accelerate the mixture rises and the available energy is kept constant, consequently the velocity of the flow is lower. The same mechanism can be applied to interpret the disparity between the CH_4 and air flow velocities considering the same fraction of CO_2.

In order to verify the simulation convergence and to ensure the conservation of the flow properties, the residual values for each discretized transport equation are presented in Table 2. All residuals for each transport equation are below 1e-3, and below 1e-6 for the energy equation.

Table 2. Residual values of each algebraic discretized equation for the multicomponent gas simulation.

Fluid	Continuity	x-velocity	y-velocity	Energy	k	Epsilon	CO2
70% CO_2 / 30% CH_4	2.3195e-04	2.1469e-05	9.5236e-06	4.9582e-07	6.8333e-05	3.3060e-04	1.2850e-16
30% CO_2 / 70% CH_4	1.6260e-04	2.4416e-05	1.0399e-05	4.8197e-07	8.1641e-05	2.5587e-04	1.1808e-16
70% CO_2 / 30% Air	1.0566e-04	3.5404e-06	1.3672e-06	2.0921e-07	3.7308e-06	5.6438e-05	1.2894e-16
30% CO_2 / 70% Air	8.4518e-05	8.4692e-06	3.8743e-06	2.4023e-07	2.9499e-05	2.7179e-04	1.5984e-16

3.2 Swirling flow

The swirl flow is applied to produce a centrifugal acceleration at the separation section where the thermodynamic condition is reached to lead the heavier components to condense. The centrifugal acceleration is used to allow the collector to remove the heavier gas components with a higher dew point by means of pushing the liquid droplets towards the nozzle upper wall.

For the numerical simulations considering swirl, the fluid is considered as methane mono-constituent and the others conditions are the same as the previous simulations. Regarding the numerical setup, the k-ω SST turbulence model was adopted due to converging problems encountered in the usage of k-ε RNG for the simulations performed with swirl.

The effects of swirls on the flow are presented in this section by imposing swirl flow at section where the vanes are installed. In order to simulate the swirl effects that vanes would generate as the domain is axisymmetric, the computational domain inlet is located in the beginning of the convergent section of the nozzle, disregarding the ellipsoid part of the central body, where the flow velocity does not have tangential component.

In this numerical analysis, the swirl velocity is imposed as a tangential component of the inlet velocity. Then, the inlet fluid velocity is set based on the vector sum of tangential and axial velocities. The swirl level is specified as the angle θ between the velocity direction and the axial component, thus, considering the velocity magnitude constant determined by the boundary conditions, an increment of the angle θ increases the tangential velocity. In addition, for the performance evaluation, the centrifugal acceleration through the supersonic separator is determined by

$$a_\theta = (V_\theta)^2/r, \tag{5}$$

being V_θ the tangential velocity and r the radial coordinate according to the axisymmetric domain.

As the swirling flow velocity increases significantly along the nozzle, at the collector outlet reversed flow is observed, not allowing to reach lower residuals concerning numerical convergence. As such, in order to avoid reversed flow at the

collector outlet, the collector length was extended from 153 mm to 306 mm, then it was possible to reach the residual values presented in the Table 3.

According to Brouwer and Epsom (2003), the centrifugal acceleration in a supersonic separator is of the order of 300,000 g to reach an appropriate rate of separation of heavier components mixed with the gas. Thus, to achieve this target, numerical simulations performed with increment in the θ angle. Since the shock wave in the supersonic separator must occur at the diffusor to ensure that gas at the upstream the collector inlet is in a thermodynamic condition that leads the heavier components to condense, and an increasing of the θ angle moves the shock wave upstream, it is needed to reduce the static pressure at diffusor outlet to balance the energy loss due to the swirl and maintain the shock wave position at the diffusor to make possible higher θ angles. Therefore, the θ angle was increased up to 60º and the static pressure at diffusor outlet was adjusted to 23 bar to reach the centrifugal acceleration of 340,000 g, as shown in the centrifugal acceleration field in Fig. 11.

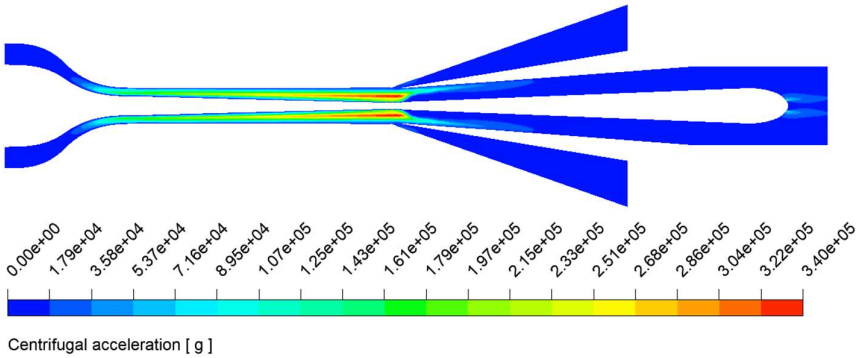

Figure 11. Centrifugal acceleration field in the supersonic separator with θ angle of 60º.

According to Wen *et al.* (2016), the vanes swirling angle of 40º to 70º generate a strong swirling flow and low temperature in the supersonic separator. Hence, the θ angle adopted in the simulations is in the range considered with a high centrifugal field and that does not reduce the expansion effect of the nozzle, which means that the low pressure and temperature condition is not weakened as a consequence of the swirling flow.

In Fig. 11, a centrifugal acceleration gradient is observed along the nozzle. In addition, a small region with an increase of the centrifugal acceleration is observed at the most downstream side of the central body around the axis, a possible explanation is that at the axis the radius coordinate tends to zero so that the centrifugal acceleration may increase locally.

As mentioned, an increasing of θ angle rises the energy loss in the supersonic separator as the swirling flow damages the expansion characteristics of the Laval nozzle due to the speed conversion from axial to tangential velocity (Wen *et al.*, 2011). The energy loss leads to the shifting of shock wave position exhibited in the static temperature variation and velocity presented along the flow centerline for the simulation considering θ angle of 60º compared with the case without swirl flow displayed in Figs. 12 and 13, respectively. As the shock wave occurs upstream in the swirl flow case, the region with low temperature and pressure for gas separation is reduced with a swirl flow.

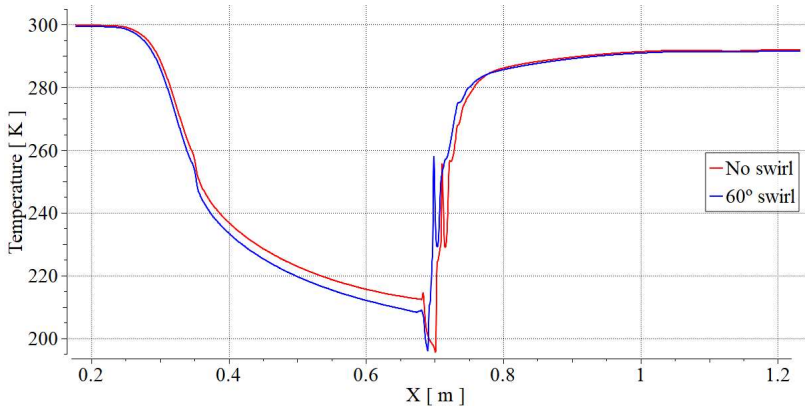

Figure 12. Static temperature along the flow centerline in the supersonic separator considering no swirl and θ angle of 60º swirling flow.

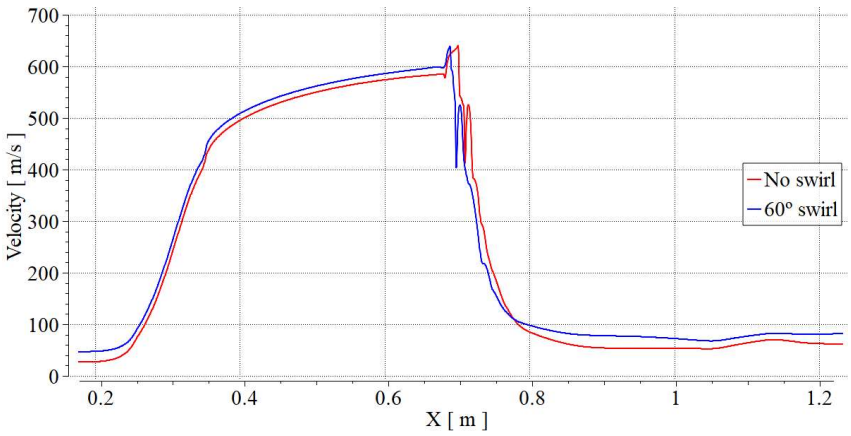

Figure 13. Velocity along the flow centerline in the separator considering no swirl and θ angle of 60º swirling flow.

In Fig. 14 and 15, the tangential velocity and the static temperature fields of the flow through the supersonic separator considering θ angle of 60º are shown, respectively. It can be verified that the region of maximum tangential velocity is located in the radial central region of the channel in the divergent section of the Laval nozzle and the peak value obtained is approximately 204 m/s. From Fig 15, it is noticed that the region with lower static temperature, around 206 K, in the divergent section is close to the central body. It can reduce the separation efficiency of the device as the liquid droplets formed in this region can re-evaporate while it is forced towards the zone adjacent to the separator wall where the temperature is elevated.

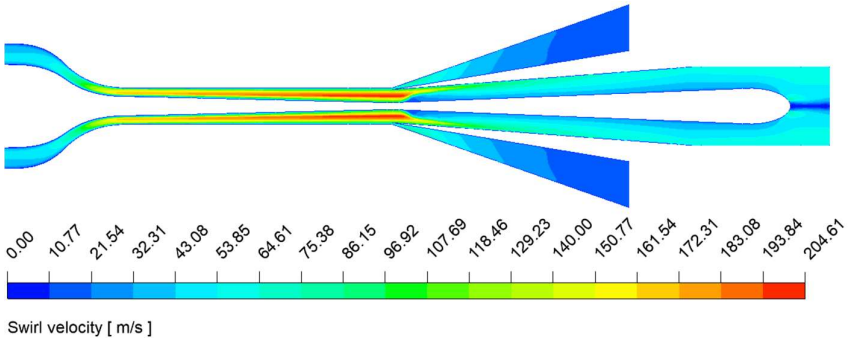

Figure 14. Tangential velocity field in the supersonic separator considering θ angle of 60º swirling flow.

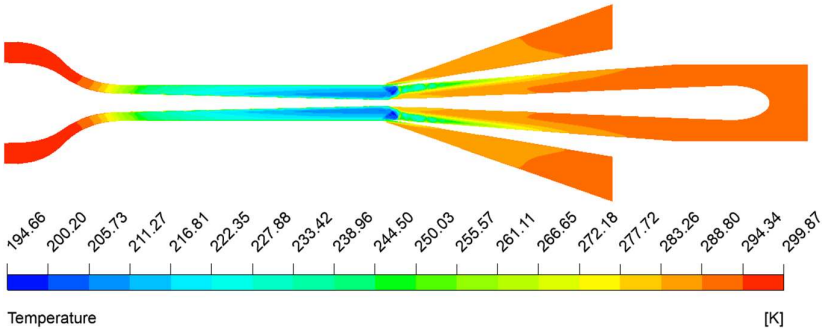

Figure 15. Static temperature field in the supersonic separator considering θ angle of 60º swirling flow.

Table 3. Residual values of each algebraic discretized equation for the swirling flow simulation.

θ	Continuity	x-velocity	y-velocity	Swirl	Energy	k	Omega
0º	7.0986e-07	2.8846e-07	2.0673e-07	-	6.6136e-08	2.7906e-07	1.4257e-05
60º	2.2011e-05	1.2045e-06	2.8623e-06	9.9035e-07	6.0016e-08	5.9719e-06	3.6341e-05

4. CONCLUSION

Numerical simulations of a supersonic nozzle considered with an asymmetrical domain and central body were carried out. Conditions with multicomponent gas were considered to identify the impact of the fluid composition variation in the flow proprieties and the results were analyzed. Regarding the simulations considering flow with swirl, it was necessary to increase the θ angle up to 60º and reduce the static pressure at the separator outlet to 23 bar in order to achieve the centrifugal acceleration which, combined with the condensation of the heavier components mixed with the gas, has an appropriate rate of separation in the supersonic separator. The changing of the boundary condition was needed to compensate the energy loss caused by the increasing of the swirl in the flow and keep the shock wave at the diffuser.

5. ACKNOWLEDGEMENTS

We gratefully acknowledge support of the RCGI – Research Centre for Gas Innovation, hosted by the University of São Paulo (USP) and sponsored by FAPESP – São Paulo Research Foundation (2014/50279-4) and Shell Brasil, and the strategic importance of the support given by ANP (Brazil's National Oil, Natural Gas and Biofuels Agency) through the R&D levy regulation.

6. REFERENCES

Ansys Inc (2019), "ANSYS Fluent Theory Guide". < https://www.ansys.com/>.

Altam, R.A., Lemma, T.A. and Juffar, S.R., 2017. Trends in Supersonic Separator design development, Universiti Teknologi PETRONAS.

Arinelli, L.O., Medeiros, J.L., Araújo, O.Q., Performance analysis and comparison of membrane permeation versus supersonic separator for CO2. Removal from a plausible natural gas of Libra field, Brazil, Offshore technology conference, OTC-26164-MS, Rio de Janeiro-RJ, 27-29 October, 2015.

Brouwer, J.M. and Epsom, H.D., 2003. "Twister Supersonic Gas Conditioning for Unmanned Platforms and Subsea Gas Processing". Offshore Europe held in Aberdeen. UK, 2-5 September 2003.

Cao, X. and Yang, W., 2015. "The dehydration performance evaluation of a new supersonic swirling separator". Journal of Natural Gas Science and Engineering, No. 27, 1667-1676.

Da Silva, I.M., Gás Natural: a sua utilização na geração de energia elétrica no Brasil, Revista de divulgação do projeto universidade Petrobras e IF Fluminense, vol.1, p.103-107, 2010.

Liu, X., Liu Z. and Li, Y., 2014. "Investigation on Separation Efficiency in Supersonic Separator with Gas-Droplet Flow Based on DPM Approach", Separation Science and Technology, 49: 2603–2612.

Matsuo, K., Miyazato, Y. and Kim, H.D., 1999. "Shock train and pseudo-shock phenomena in internal gas flows". Progress in Aerospace Sciences, No. 35, p. 33-100.

Menter F.R., 1994. "Two-Equation Eddy-Viscosity Turbulence Models for Engineering Applications". AIAA Journal, 32 (8), 1598-1605.

Redlich, O., Kwong, J. N. S., 1949. "On the Thermodynamics of Solutions". *Chem. Rev*. 44 (1): 233–244

Twister, Supersonic Gas Solutions. "Twister supersonic separator - How it works". 21 Sep. 2017 <http://twisterbv.com/products-services/twister-supersonic-separator/how-it-works/>.

Vesteeg, H. K. and Malalasekera, W., An introduction to computational fluid dynamics - the finite volume method. [S.l.]: Addison-Wesley-Longman, 2007.

Wang, Y. and Hua, D., 2018. "Structure improvements and numerical simulation of supersonic separators with diversion cone for separation and purification". *Journal of The Royal Society of Chemistry*, No. 8, p. 10228–10236

Wen, C., Li, A., Walther, J.H., Yang, Y., 2016. "Effect of swirling device on flow behavior in a supersonic separator for natural gas dehydration". *Separation and Purification Technology*, No. 168, p 68–73.

Wen, C., Xuewen, C., Yang T. and Zhang J., 2011. "Swirling Effects on the Performance of Supersonic Separators for Natural Gas Separation". *Chemical Engineering Technology*, No. 9, p. 1575–1580.

Wylen, V., 1998. "Fundamentals of Thermodynamics – Fifth Edition".

Yakhot, V., Orszag, S.A., Thangam, S., Gatski, T.B. and Speziale, C.G., 1992. "Development of turbulence models for shear flows by a double expansion technique", Physics of Fluids A, Vol. 4, No. 7, pp1510-1520.

Yang, Y., Wen C., Wang and S. Feng, Y., 2014. "Numerical simulation of real gas flows in natural gas supersonic separation processing". *Journal of Natural Gas Science and Engineering*, No. 21, p. 829-836.

7. RESPONSIBILITY NOTICE

The authors are the only responsible for the printed material included in this paper.